Nanoscale

PAPER

View Article Online
View Journal | View Issue

Cite this: *Nanoscale*, 2026, **18**, 5564

Multiexciton absorption cross sections of CdSe@CdS nanorods studied using pump–repump–probe spectroscopy

Krishan Kumar, *†[a,b] Jens Uhlig, [c,d,e] Raktim Baruah,‡[a,b,f] Shivani Yadav[a,f] and Maria Wächtler *‡[b]

Received 25th November 2025,
Accepted 6th February 2026

DOI: 10.1039/d5nr04981d

rsc.li/nanoscale

While the multiexciton dynamics in semiconductor nanocrystals is widely explored, to determine the absorption cross sections for multiexcitons of varying order is still a challenge. In this study, we performed pump–repump–probe transient absorption (ppp-TA) spectroscopic measurements on CdSe@CdS nanorods to gain insights into the absorption cross sections for multiexcitons. By tuning the pump–repump delay time and repump intensity, we were able to generate and reexcite various transiently living multiexcitonic species distributions. By modelling the ppp-TA data using a Markov Chain Monte Carlo target analysis method, the spectral shape and lifetime of higher order excitons (up to tri-excitons), and absorption cross section parameters for different multiexcitonic species are accessible. We find that at the repump wavelength 400 nm used in this study the absorption cross sections of the exciton and multiexciton species are smaller compared to the ground state species. The determined values indicate that the biexciton absorption cross section at 400 nm is slightly larger than the cross section for the monoexciton and triexciton determined in our study.

Introduction

Semiconductor nanocrystals have been widely explored due to their size-tuneable optoelectronic properties governed by the quantum confinement effect, which make them excellent candidates for applications such as photocatalysts, light-emitting diodes, solar cells, and many more.[1–7] The absorption of photons of suitable energy by the nanocrystals generates a bound electron–hole pair known as an exciton. At intense excitation conditions, *i.e.*, at a high flux of photons, multiple interacting excitations can be generated in a single nanocrystal by absorption of several photons by the same nanoparticle.[8,9] These multiple interacting excitons are called biexciton (2 e–h pairs), triexciton (3 e–h pairs), *etc*. They are of significant interest for applications, *e.g.*, in nanocrystal based lasers or solar cells with efficiencies exceeding the Shockley–Queisser limit.[5,10,11]

The distribution of excitons and multiexcitons generated by absorption of several photons in dependence on excitation intensity is usually described by Poissonian statistics, which depends on the number of photons per unit area incident on the nanocrystal and the absorption cross sections.[8,12,13] However, the absorption cross section of nanocrystals governing the formation of multiexcitons is complex. For the absorption cross section two models are discussed in the literature: First, the absorption cross section is considered independent of exciton order due to the availability of a large number of electronic states that can be populated upon excitation, which is termed as constant absorption cross section model. *E.g.*, intensity dependent transient absorption studies often assume constant absorption cross sections to determine the population of higher order excitons using Poisson distribution.[8,12,13] This model is also used in multiexciton generation efficiency calculations, where only the ratio of transient signal at early time delays and long time delays are

[a]*Department Functional Interfaces, Leibniz Institute of Photonic Technology Jena, Albert-Einstein-Straße 9, 07745 Jena, Germany.*
E-mail: krishan.kumar@uni-oldenburg.de
[b]*Chemistry Department and State Research Center OPTIMAS, RPTU Kaiserslautern-Landau, Erwin-Schrödinger-Str. 52, 67663 Kaiserslautern, Germany.*
E-mail: waechtler@phc.uni-kiel.de
[c]*Division of Chemical Physics, Department of Chemistry, Lund University, Box 124, SE-22100 Lund, Sweden*
[d]*NanoLund, Lund University, 22100 Lund, Sweden*
[e]*LINXS Institute of Advanced Neutron and X-Ray Science, Lund University, 22370 Lund, Sweden*
[f]*Institute of Physical Chemistry, Friedrich Schiller University Jena, Lessingstraße 8, 07743 Jena, Germany*
†Current address: Institut für Physik, Carl von Ossietzky Universität, Carl-von-Ossietzky-Straße 9-11, 26129 Oldenburg, Germany.
‡Current address: Institute of Physical Chemistry and Kiel Nano, Surface and Interface Science (KiNSIS), Christian-Albrechts-Universität zu Kiel, Max-Eyth-Straße 1, 24118 Kiel, Germany.

considered.[14,15] Second, the absorption cross section is discussed to change with exciton order due to filling up specific electronic levels resulting in blocking that particular transition due to the Pauli exclusion principle. This model is termed state-filling model.[16] *E.g.*, for a doubly degenerate system like the $1S_e$ electronic levels of CdSe nanocrystals involved in the lowest energy excitonic transition, the absorption cross section of the band edge transition is expected to reduce by half after monoexciton formation, and it is expected to reduce to zero after biexciton formation. For CdSe and (CdSe)ZnS core–shell quantum dots, the absorption cross sections of higher-order excitons have been shown to follow the qualitative description of the state-filling model when probed close to band-edge for small quantum dots while constant absorption cross sections are observed for large quantum dots when probed above the band edge.[16] Further, in dependence on the excitation conditions different cross sections are discussed by Tahara *et al.*[17] Band-edge re-excitation experiments using pump–repump–probe transient absorption (ppp-TA) spectroscopy with the repump energy corresponding to the bandgap have shown reduced absorption cross sections for the generation of bi- and tri-excitons from the monoexciton state compared to the absorption cross section for the transition from the ground to monoexciton state in the case of spherical PbS/CdS core/shell nanocrystals. In contrast to the generation of multiple excitons by two consecutive temporally separated pump pulses, under simultaneous excitation the absorption cross sections are treated to be the same in this study. The authors in this study used single wavelength analysis to show that these difference in the absorption cross sections under different excitation conditions, *i.e.,* generation of higher order excitons with only one excitation pulse in normal pump–probe transient absorption experiments (pp-TA) and generation of higher-order excitons by consecutive, temporally separated pulses by re-excitation in a ppp-TA experiment, originated from excitonic coherences between monoexciton and multiexcitons in the case of simultaneous absorption of multiple photons in the excitation intensity dependent studies applying one excitation pulse. Under consecutive excitation in multi-pulse excitation schemes, *e.g.*, in ppp-TA spectroscopic studies, coherences don't exist anymore and state filling effects on the absorption cross section can be observed at the band edge transitions. This survey on results in literature illustrates the challenge in evaluating absorption cross section of excitons and multiexcitons which depend apparently strongly on excitation conditions, *i.e.* band-edge *vs.* above band-edge or simultaneous (coherent) excitation *vs.* consecutive steps.

The basis to modelling multiexciton dynamics and a challenge in determining absorption cross sections is to monitor reliably the distribution of multiexciton species in the experiment, which allows to calculate back on the initial populations upon excitation and hence allows to derive values for the absorption cross sections. A precondition for a proper analysis of multiexciton behavior and determination of their absorption cross sections is that the exciton order is identified spectroscopically. However, in single probe analysis, the absence of unique spectral features makes it challenging to correctly assign the order of exciton that is generated. Global analysis of intensity-dependent broadband transient absorption data could help solve this issue. Recently, spectral signatures of multiexcitons in CdSe quantum dots[18,19] and CdSe@CdS nanorods, heterostructures consisting of a spherical CdSe core embedded within a 1d rod-shaped CdS shell,[20] have been reported using sampling of experimental pp-TA data to a target model by a MCMC approach,[21] which can allow reliable exciton order assignment. *E.g.*, the modelled data showed that the disappearance of the photoinduced absorption (PA) signal in higher energy spectral region can be associated with the multiexciton formation in CdSe@CdS nanorods.[20] This information forms the basis for the qualitative determination of multiexciton formation and distributions in the pump–repump transient absorption experiments for CdSe@CdS nanorods reported here.

In this contribution we investigate the absorption cross sections of various transiently living excitonic and multiexcitonic species of heterostructured CdSe@CdS nanorods using intensity dependent pump–repump spectroscopy. The heterostructured system were chosen to test our approach, because they possess clearly distinguishable spectral signatures for mono and multiexcitonic states compared to simple *e.g.,* CdSe quantum dots as was demonstrated in previous studies.[18–20] Tuning the time delay between pump and repump pulse allows to target different higher-order exciton distributions. The global modelling of ppp-TA data allows to simultaneously determine the spectral and dynamical features of multiexcitons, as well as the determination of respective absorption cross sections of various multiexcitons. This allows us to extend the comparison of absorption cross sections of the ground state and monoexcitonic species to absorption cross sections of higher order excitons at the chosen excitation wavelength.

Results and discussion

The CdSe@CdS nanorods used in this study with quasi-type II band alignment (length 20.1 ± 1.6 nm, width 4.7 ± 0.7 nm, seed size 2.3 nm) were synthesized following the well-established seeded-growth approach.[22,23] The absorption spectra and transmission electron microscopic images of as synthesized nanorods are presented in Fig. S1. We used pump–repump–probe spectroscopy to understand the multiexciton generation properties and the absorption cross sections for higher-order excitons generated by sequential pump excitation. In our experiment, both excitation pulses were chosen to have 400 nm central wavelength, hence we work under above band excitation conditions, and a pulse duration of ~100 fs. To ensure sufficient signal contribution of species in the ensemble that has interacted with both excitation pulses, the intensity of the first pump pulse was set to >750 μJ cm^{-2}, sufficiently high to excite a significant part of the ensemble. Multiexcitons generated at this high fluence decay sequentially *via* the Auger recombination process.[8,20] The choice of the delay between the two pump pulses is crucial to determine the

species that are interacting with the second pump pulse and, hence, are re-excited. The schematic illustration of the consecutive excitation scheme is presented in Scheme 1. To target mainly monoexciton species, the delay between the two pump pulses needs to be set longer than the Auger recombination decay lifetime of the higher-order multiexcitons in the CdSe@CdS system to give sufficient time for all the higher-order multiexcitons to decay forming a monoexciton population. This selectively allows us to investigate the cross section of the monoexcitons in the system. In case of shorter delay times, a complex mixture including higher-order excitons will be re-excited. The intensity of the repump pulse is chosen for our experiments spanning a range of low intensity, ensuring that multiexcitons can only generated from interaction with both pump pulses, to high intensities allowing to produce also significant amounts of higher-order excitons upon interaction with the second pump pulse. From the gradual development of spectral signatures and kinetics of the double-excited system in experiments with varying intensity of the second pump pulse, the combination of sufficiently distinguishable decay lifetimes, and the extracted absorption cross section of lower order excitons allowed us to estimate the absorption cross section of subsequent higher order multiexcitons.

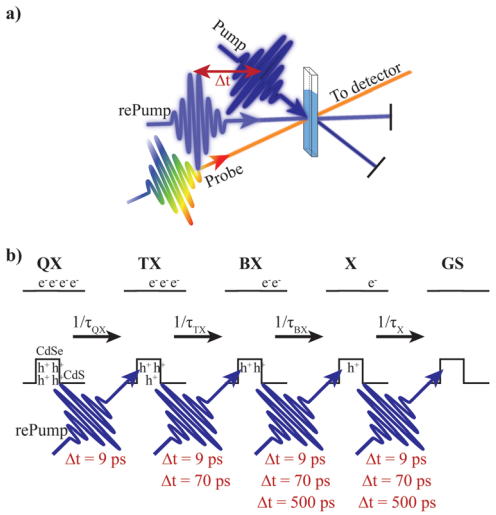

Scheme 1 Schematic description of pump–repump–probe transient absorption (ppp-TA) spectroscopy. (a) Pump sequence used in the ppp-TA experiment. (b) The sequential decay of multiexciton species generated by the first pump pulse and targeted re-excited species as a function of delay between the two pump pulses (Δt). τ are the Auger recombination lifetimes of the multiexciton species QX, TX, BX, X, and GS, which represent the tetra-, tri-, bi-, monoexciton, and ground state, respectively.

In the first step, to mainly target monoexciton re-excitation, a time delay between the pump and repump pulse of 500 ps was set which is much longer than the biexciton lifetime in CdSe@CdS nanorods of ~160 (ref. 24)–180 ps.[20] The repump intensity dependent ppp-TA spectra of CdSe@CdS nanorods with 502 ps delay (*i.e.*, after 2 ps of excitation with the repump pulse) are shown in Fig. 1a in direct comparison with a spectrum at 502 ps without repump-excitation (pp-TA) of the sample (see also Fig. S2). The pp-TA spectrum (Fig. 1a, blue curve) shows strong negative features at 455 nm and a weak negative signal at 553 nm corresponding to the bleach of the lowest excitonic transitions localized in the CdS and the CdSe domains, respectively, of the seeded nanorods caused by the state filling effect.[12,25] Additionally, a photoinduced absorption band is also present at 423 nm, which has been assigned to the carrier-induced Stark effect in the monoexciton species, also known as biexciton effect.[8] The sign of the PA band allows to directly distinguish between the monoexciton and multiexciton species, because only a monoexciton interaction with the probe pulse would result in a positive signal, whereas multiexciton formation would lead to loss of this signal or even form a negative signal.[20] Thus, this band provides a clear spectroscopic handle to observe the influence of repump interaction in the ppp-TA data. Upon excitation with the repump pulse, the TA spectra show an increased CdS band-edge bleach at 455 nm (see Fig. S3), and the

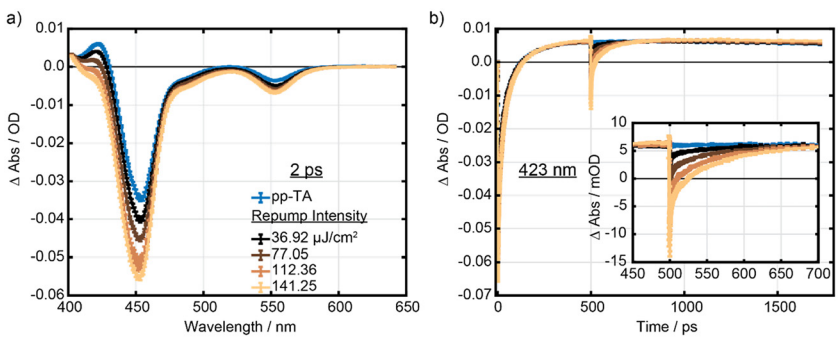

Fig. 1 ppp-TA data of CdSe@CdS nanorods dispersed in toluene. A time delay of 500 ps is set between both pump pulses with a central wavelength of 400 nm. (a) Second pump (repump) intensity dependent TA spectrum of nanorods at 2 ps after the arrival of the second pump pulse (black to light brown traces). For comparison, a representative pp-TA spectrum (first excitation pulse only) of CdSe@CdS nanorods is plotted at 502 ps (blue curve), *i.e.* 2 ps after interaction with the repump pulse. The intensity of the first pump was 791.33 μJ cm^{-2}. (b) ppp-TA kinetics of the PA band at 423 nm with varying re-excitation intensity as shown in the legend, along with representative pp-TA kinetics of the same band shown in blue (pump intensity 791.33 μJ cm^{-2}). The inset shows the magnification near the re-excitation event.

intensity of the PA band around ~423 nm is decreased (Fig. 1a, black curve). Also, the CdSe bleach signal at 553 nm increases with increasing repump intensity (Fig. 1a and Fig. S3). The increase in bleach signals with simultaneous decreases in the PA band can be directly associated with the formation of biexcitons or even higher-order exciton species.[24,26–28] With increasing intensity of the repump pulse, the changes in the TA spectral shape get more pronounced. To observe the transient kinetic changes upon repump interaction and the decay of multiexcitons, we use the 423 nm PA band as an indicator[20] for the formation of multiexcitons with and without repump-excitation. The kinetic profiles at 423 nm (Fig. 1b) close to time zero (1st pump excitation) immediately show a negative signal, in accordance with the direct formation of multiexcitons from the intense pump excitation. The transient signal then decays to a positive signal representing the decay of all higher-order excitons to the monoexciton state before the interaction with the repump pulse at 500 ps. Upon interaction with the repump pulse, the kinetic traces of the 423 nm PA band show an immediate reduction (or less positive signal) compared to the pump-only trace, which recovers to form a positive signal again within a few 100 ps. This negative deviation can even be observed when the repump intensity is sufficiently low and generates only monoexcitons upon interaction with not preexcited nanorods (see Fig. S2 repump-only TA data, black trace). Hence, ground state excitation, if present, with the repump pulse would result in monoexciton formation, which would result in a net increase in positive signal after interaction with the repump pulse. The negative deviation observed after repump though relates to the formation of multiexcitons, and that can only occur upon re-excitation of monoexcitons in the ensemble under low re-pump intensity conditions. Higher intensity of the repump pulse results in a stronger reduction in the PA signal due to increased likelihood of re-excitation and additionally increasing contributions from multiexciton formation directly by ground state excitation (see Fig. S2). The subsequent decay of the negative deviation in 423 nm kinetics (Fig. 1b) is due to the Auger recombination of multiexciton to form mono-exciton again.[20]

To quantitatively model the data, we used the Markov Chain Monte Carlo (MCMC) sampling method for target analysis.[21,29] The MCMC algorithm can be helpful in determining robustness of the used target model compared to a Levenberg–Marquardt or a trust region optimization algorithm by looking at the posterior probability of parameter pairs. The MCMC algorithm determines the posterior probability, $P(\theta|x)$, that a certain set of parameters θ, describes the observed data x, using the Bayes' theorem. Since we are not interested in the absolute probabilities, only the relative probabilities that a given set of parameters define the observed data, for our purpose the posterior probability can be defined as $P(\theta|x) \sim P(x|\theta)P(\theta)$, where the first term is the likelihood and the second term is the "prior" representing the prior knowledge about the system. In our case, we have used prior information that a probability distribution exists within the given limits only and is zero outside these limits.[21,29] For CdSe@CdS nanorods an extended Auger recombination model involving additional surface state trapping has been suggested,[20] which under our experimental conditions involving high excitation intensity of the first pump pulse reduces to the standard quantized sequential cascade non-radiative Auger recombination model to describe the experimental data.[30,31] A kinetic model comprising four exciton species (since a minimum of up to tetraexciton contributions was required to describe intensity dependent pp-TA data of CdSe@CdS in the intensity range up to 930 μJ cm^{-2}) is shown in Fig. 2a.[20] The experimental data was modelled in the time range between 2 and 1000 ps with respect to the first pulse excitation. This time window has been chosen to focus on the Auger recombination processes and remove the sub-ps fast exciton cooling and hole-localization driven exciton localization processes of the initially in the CdS domain generated excitons to form excitons with the hole localized in the CdSe seed and the electron delocalized over the CdS shell, according to the quasi-type II band alignment in our system, interfering with the observed multiexciton decay dynamics at delay times below 2 ps.[32,33] For the same reasons, the time window close to repump excitation (499–502 ps) has also been neglected. The obtained experimental data can be understood as a classical pp-TA data set before the arrival of repump pulse, *i.e.*, up to 499 ps, with excitation of ground state species solely generating a distribution of excitons and multiexcitons. To describe the initial distribution of population after excitation under our excitation conditions a Poisson distribution is used. We follow here the argumentation that although the lowest band edge states in CdSe and CdS systems show only low degeneracy and application of Poisson distribution is questionable upon band edge excitation, with excitation above band edge high number of states for excitation are available and situation similar to excitation of highly degenerate systems are found.[18,34] Further, due to coherent excitation within the pulse width, coherences between monoexciton and multiexcitons in the case of simultaneous absorption of multiple photons levelling out potential differences in absorption cross sections for the individual excitation steps leading to higher-order excitons.[17] Hence, the requirements for application of Poisson distribution are fulfilled. The Poisson distribution is dependent on the excitation intensity and the ground state absorption cross section σ_1 (see eqn (S3) SI) in this case. The σ_1 parameter was fixed to a value previously determined for CdSe@CdS nanorods in an experiment covering a similar intensity regime as the first pump intensity in our ppp-TA data analysis.[20] After re-excitation with the repump pulse the change in population distribution at repump delay time needs to be re-modelled due to interaction of the re-pump pulse with all species present in the ensemble at that specific delay time. In the case of a pump–repump delay of 500 ps the transient species of interest would be mainly monoexciton and the ground state species. The re-excitation of is modelled generating a Poisson distribution of populated states for each species individually, once taking the not excited particles as starting point, and second taking the monoexciton as starting point. The arguments for using Poisson distributions to describe these excitations is the same

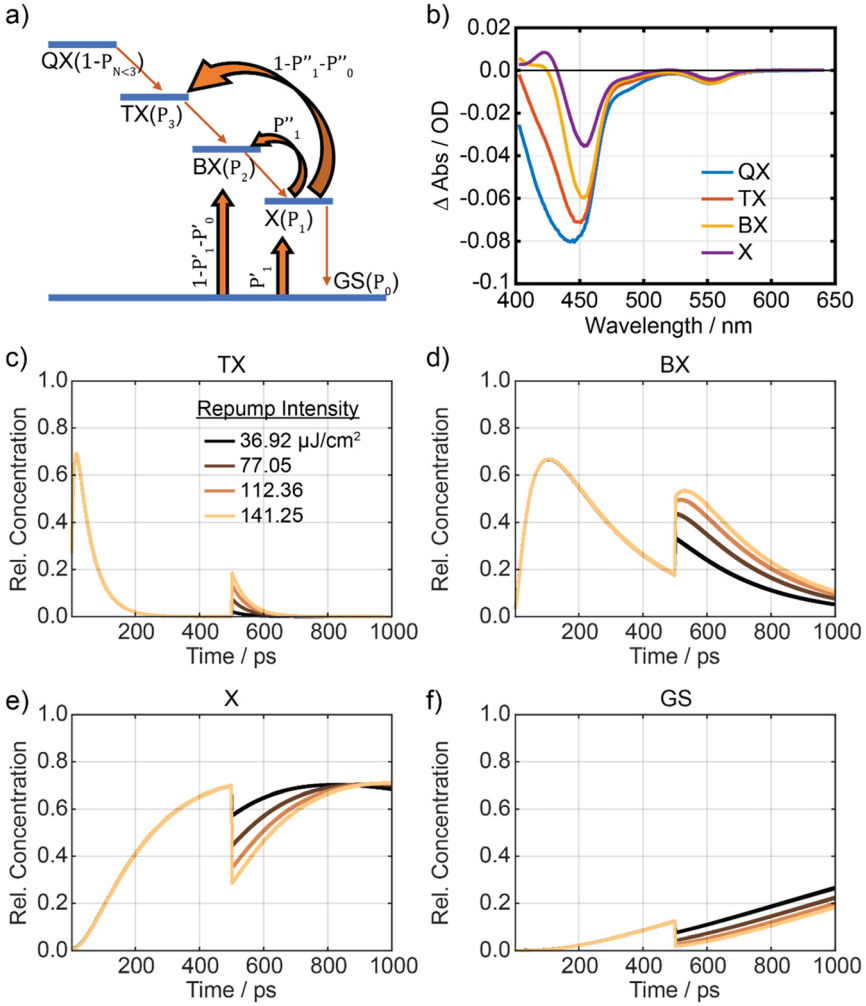

Fig. 2 Results of Markov Chain Monte Carlo (MCMC) modelling of pump–repump–probe transient absorption data with 500 ps pump–repump delay. (a) Kinetic model used to sample the whole ppp-TA experimental data (starting from 2 ps of first pump pulse excitation to 1000 ps). The first pump pulse generates the excited population of species which decay *via* Auger recombination as shown by the thinner downward pointing arrows and after 500 ps the relevant re-excitation contributions are shown by the thicker upward moving arrows. The initial population distribution of species by the first pump pulse is shown in brackets, which are dependent on σ_1 (known) and re-excited fractions for GS and X are dependent upon the modelled σ_{GS} and σ_X parameters respectively. Further details on the kinetic model are given in SI. (b) Species-associated spectra of modelled multiexcitons. (c–f) Relative concentration decay profiles of modelled tetra-, tri-, bi-, mono-exciton and ground state species, respectively. The repump intensities are given in the legend and colour scheme is kept consistent for panel c–f. Each curve is plotted from 100 random samples drawn from the MCMC chain.

as before: it is an independent excitation of these species by one excitation pulse and we use a pump pulse centered at 400 nm which is significantly above the band-edge and a high number of states are available for re-excitation events. Hence, the re-excitation can be regarded similar to the interaction of the first pump pulse, just meeting an ensemble containing two species, the non-excited nanorods and the nanorod which were excited and now hosting a monoexciton. Hence two free absorption cross section parameters for the monoexciton (σ_X) and the ground state species (σ_{GS}) must be considered for the re-excitation event. The loss of the excited ensemble by stimulated emission induced by the repump pulse can be neglected as it is not resonant with the band-edge emission. Further details on the kinetic modelling are given in the SI.

Detailed modelling results, including species-associated spectra, relative concentration profiles of various species, are shown in Fig. 2b–f. Corner plots and kinetic fits can be found in the SI (Fig. S4 & S5). The resulting lifetimes of various exciton species (Table 1) match well with the previously estimated lifetimes for CdSe@CdS nanorods.[20,24] The lifetime of the biexciton calculated here is ~256.5 ps, which is slightly higher compared to the literature-reported values of 160 (ref. 24)–180 ps.[20] The species-associated spectra obtained from the Markov Chain (Fig. 2b) are in agreement with the results derived from pump-intensity dependent TA pp data and show the characteristic disappearance of the PA band and increasing bleach contributions for higher-order excitons. The band-edge bleach contribution of the CdS domain increases with exciton order (X, BX, TX and

Table 1 Fitted median values and 95% confidence intervals extracted from MCMC sampling for intensity-dependent pump–repump–probe spectroscopy of TOPO capped CdSe@CdS nanorods. The absorption cross section value, $\sigma_1 = 4.14 \times 10^{-15}$ cm^2,[20] for the interaction with the first pump pulse has been kept constant and the absorption cross sections for repump excitation of ground state σ_{GS} and monoexciton state σ_X are modelled as free parameters for monoexciton re-excitation (500 ps). The obtained σ_{GS} and σ_X are then used for biexciton re-excitation 70 ps data evaluation and likewise σ_{GS}, σ_X, and σ_{BX} are given as fixed parameters for triexciton re-excitation (9 ps) data evaluation as detailed in SI

Parameter name		Monoexciton re-exc. (500 ps)	Biexciton re-exc. (70 ps)	Triexciton re-exc. (9 ps)
$\tau_{tetraexciton}$/ps[a]		$7.30^{7.35}_{7.25}$	$7.66^{7.68}_{7.65}$	$4.31^{4.38}_{4.25}$
$\tau_{triexciton}$/ps		$49.04^{49.32}_{48.76}$	$41.89^{42.00}_{41.79}$	$35.45^{35.77}_{35.15}$
$\tau_{biexciton}$/ps		$256.5^{254.4}_{258.7}$	$231.8^{232.6}_{231.1}$	$188.6^{190.3}_{187.0}$
$\tau_{monoexciton}$/ps[b]		1772^{1787}_{1756}	2459^{2478}_{2448}	2109^{2126}_{2092}
Abs. cross section ($\sigma \times 10^{-15}$)/cm^2 (repump)	σ_{GS}[d]	$6.73^{6.75}_{6.71}$	6.73[c]	6.73[c]
	σ_X	$3.63^{3.65}_{3.61}$	3.63[c]	3.63[c]
	σ_{BX}	—	$5.05^{5.06}_{5.04}$	5.05[c]
	σ_{TX}	—	—	$3.75^{3.80}_{3.72}$

[a] Includes contributions of higher order excitons which are not explicitly modelled. [b] Represents out-of-modelled time window values. [c] Represents constant values used in modelling the respective experiment. [d] σ_1 and σ_{GS} in principle representing the same absorption cross section vary slightly in their values. To reduce the number of free running parameters, σ_1 was set to a value determined form a pump-intensity dependent experiment using only pump 1. Only σ_{GS} was optimized for the presented dataset and determined from the data sets with varying intensity of the second pump. The comparisons made in this manuscript are between cross sections determined from the changes in the TA data caused by the second pump and are referenced to the absorption cross section determined from the second pump. Hence the trends reported for σ_{GS}, σ_x, σ_{BX}, σ_{TX} are representative.

QX). Contrary to expectation by state-filling, the CdS band-edge bleach of monoexciton spectra is slightly more than half (60%) of the biexciton spectra, which has been shown to be the case in cadmium-based nanoparticles.[26,35]

The relative concentration decay profiles of triexciton (TX), biexciton (BX), monoexciton (X), and ground state (GS) obtained by sampling ppp-TA experimental data are presented in Fig. 2c–f, respectively. The concentration profile for tetraexciton (QX) is given in the SI (see Fig. S4). The modelled concentration profiles show that the pre-formed monoexciton concentration reduces (see Fig. 2e) and increases for biexciton (Fig. 2d) and triexciton (Fig. 2c) upon repump excitation, showing the formation of higher order excitons from the X species. The relative concentration of the ground state also decreases, indicating partial excitation of the GS by the repump pulse (Fig. 2f). As expected, the higher the intensity of the repump pulse is, the higher the reduction in X and GS concentration, which gets converted to higher-order excitons. Important to note is, that according to the results of the model, the absorption cross section of the monoexciton state is reduced by ~46% compared to the absorption cross section of the corresponding ground-state (Table 1).

Reducing the time delay between the two-pump pulses could allow the re-excitation of biexciton and triexcitons in the ensemble respectively and hence, potentially allow also the estimation of absorption cross section of these transiently living higher-excitonic species. We tested this approach in a ppp-TA experiment to extract additional information on the biexciton re-excitation process. Since the lifetime of the biexciton estimated by ppp-TA modelling is ~257 ps and of the triexciton is 50 ps, for this experiment, we reduced the delay between both pump pulses to 70 ps. This delay was chosen so that most of all the higher-order excitons (QX and TX) formed directly by the absorption of intense first pump pulse would have decayed significantly allowing us to mainly target the BX, X and GS species remaining in the ensemble for re-excitation, though GS species can be neglected at 70 ps repump delay (Fig. 1f). The ppp-TA spectra show higher bleach intensity at the CdS band-edge and in the 423 nm region upon excitation with the repump pulse (Fig. 3a) compared to the pp-TA spectra at 72 ps (Fig. 3a, blue curve and Fig. S6). The ppp-TA kinetics at the PA feature at 423 nm also shows that the interaction of repump pulse increases the bleach signal compared to the pp-TA first pump only kinetics (Fig. 3b), which recover to a posi-

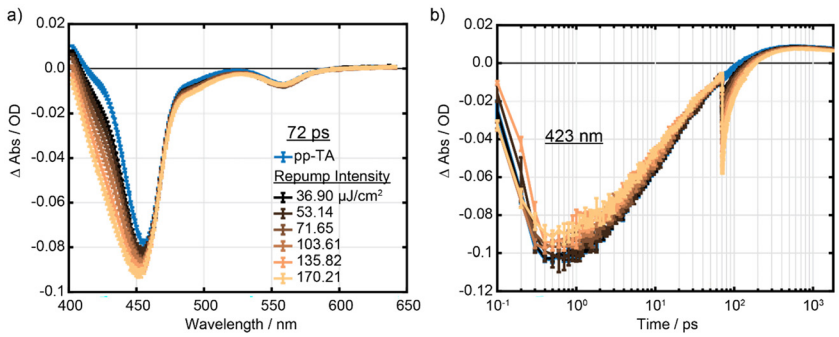

Fig. 3 ppp-TA of CdSe@CdS nanorods for biexciton re-excitation. A 70 ps time delay between the pump and repump pulse is kept constant. (a) Repump intensity dependent ppp-TA spectrum at 2 ps after the second pump excitation (*i.e.* 72 ps after first pump excitation). For comparison, the pp-TA spectrum of CdSe@CdS nanorods after 72 ps of excitation with the first pump pulse intensity 1071.86 μJ cm^{-2} (blue curve). (b) ppp-TA kinetics at 423 nm with increasing second pump intensity (black to light brown curve). Representative pp-TA kinetics without the repump pulse is shown by blue curve for comparison.

tive signal over the course of the following ~200 ps. These changes in the transient signal get stronger with increasing repump intensity. Furthermore, the band-edge bleach of the CdS domain also increases with repump interaction while the bleach signal in the CdSe domain does not change significantly (Fig. S7). These observations are consistent with the formation of higher-order excitons by the interaction of repump pulse with the BX and/or X species.

To mathematically model the experimental data, we used the above kinetic model with four excited species as well in the time range between 2 and 1000 ps with respect to the first pulse excitation and further the time region for 69–72 ps have been ignored as described previously. To avoid too many free parameters, which could potentially result in complex dependencies, we fixed the absorption cross section of X, and GS obtained from previous MCMC fits and fit only the absorption cross section for BX. The lifetime obtained are in very good agreement with the values determined from X re-excitation with a pump repump delay of 500 ps, see Table 1. The corner plot and species-associated spectra obtained from MCMC sampling of the experimental data are given in SI (see Fig. S8 and S9). The relative concentration profiles of the modelled exciton species are presented in Fig. 4. The concentration profiles of X and BX show a decrease upon repump excitation, whereas the concentration profiles of TX and QX show a simultaneous increase, which quantitatively shows the formation of higher order excitons (QX, TX) from BX and X upon excitation with repump pulse at 70 ps delay time. The MCMC sampling of the experimental data allows the calculation of the absorption cross section for BX, which is with a value of 5.05×10^{-15} cm^{-2}, ~25% lower compared to the ground state absorption cross section (Table 1).

Inspired by the results of monoexciton and biexciton re-excitation experiments, we finally further reduced the delay between the two pump pulses to 9 ps to also target the re-excitation of TX to higher-order excitons. The experimental ppp-TA spectra obtained by repump excitation is presented in Fig. S10a, and the single pulse pp-TA data is given in SI (Fig. S11). The transient spectra show only a slight increase in bleach intensity in the CdS nanorods region and the position of the PA signal at 423 nm. The kinetic trace at 423 nm of the ppp-TA data (Fig. S10b) illustrates the recovery of some ground state absorption (increased bleach) introduced by the repump pulse. Similar change in kinetics of 455 nm, CdS band-edge bleach is observed, while the kinetics of the CdSe band-edge bleach at 553 nm, do not show any significant changes in TA signal after repump interaction (see Fig. S12). We modelled this ppp-TA experimental data in 2–1000 ps with respect to first pump pulse and ignoring the data around the repump pulse between 8–11 ps using a similar kinetic model with additional TX re-excitation parameters along with the fixed re-excitation absorption cross section of the rest of the species as obtained from the previous ppp-TA MCMC sampling. The corner plot of the fit parameters, concentration profiles, and the kinetics fit sampled by MCMC are given in SI (Fig. S13–S15). The lifetimes of modelled species (Table 1) are compar-

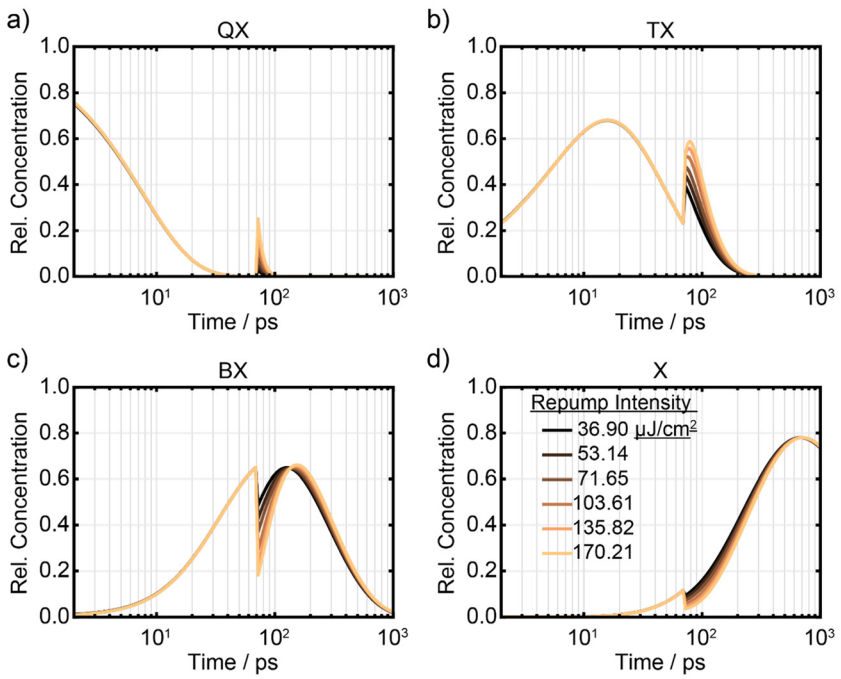

Fig. 4 MCMC modelling of bi-exciton re-excitation experiment with a delay between two pump pulses of 70 ps. (a–d) Relative concentration decay profiles of modelled tetra-, tri-, bi-, mono-exciton, respectively, with increasing repump pulse intensity. The relative concentration of ground state species is shown in SI. Each curve is plotted from 100 random samples drawn from the MCMC chain.

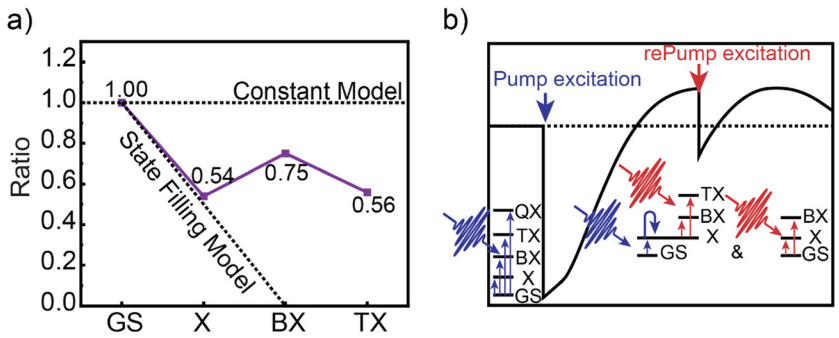

Fig. 5 (a) Absorption cross section ratio for higher-order excitons normalized to ground-state absorption cross section estimated using ppp-TA. (b) Schematic showing the multiexciton generation events in ppp-TA experiments leading to observed differences in the absorption cross section.

able to the previously obtained values. The TX absorption cross section is 3.75×10^{-15} cm^{-2} which is ~44% less compared to ground state absorption cross section value. These changes in absorption cross section are shown in Fig. 5a.

Discussion and conclusions

In summary, we performed ppp-TA experiments with varying delays between pump and the repump pulse. We determine the absorption cross section of higher-order excitons at the excitation wavelength by modelling the intensity dependent ppp-TA data for CdSe@CdS nanorods. Under our experimental conditions we observe that the absorption cross sections at 400 nm in our system for mono-, bi- and triexciton are smaller than for the not excited nanorods. For the different (multi)-excitonic species the absorption cross sections vary slightly. A similar result has been obtained for PbS/CdS core/shell system where the absorption cross section for the not excited systems is found to be larger than the absorption cross section of the monoexciton.[17] Interestingly, for our systems the BX absorption cross section appears to be higher compared to other transiently living species such as X and TX but still lower than the GS absorption cross section. For a detailed understanding of these trends in the absorption cross sections at the investigated wavelength of 400 nm support from theoretical modeling will be necessary. Our results show, that generalizing the behavior to follow either the constant absorption cross section model or the state filling model is not reflecting the trends for changes in the absorption cross sections between these different species, especially upon above band-edge excitation. In some way our data could be discussed that the drop in absorption cross section from the ground state system to the excited system is related to state-filling effects, while in the cross sections of the excited systems the constant cross section model seems more valid, justified by a high density of higher energy levels available for further excitation in our system. Furthermore, we expect that these results are directly transferable to Cd-based nanorods, since the multiexcitonic properties of CdS and CdSe@CdS nanorods have been shown to follow similar behaviour.[20]

Experimental

All the chemicals and solvent used in the synthesis of CdSe@CdS nanorods and CdS nanorods were purchased from Sigma Aldrich (Merck KGaA, Darmstadt, Germany) except for octadecyl phosphonic acid (ODPA), which was purchased from Carl Roth GmbH + Co. KG (Karlsruhe, Germany) and used without further purification. The solvents toluene and methanol used were dry, deoxygenated, and of spectroscopic grade.

CdSe seeds were synthesized using a previously established protocol.[36] CdO (61.1 mg), ODPA (~0.29 g) and trioctylphosphine oxide (TOPO, 3 g) were mixed in a three-neck flask and heated to 150 °C under constant stirring and evacuated for 30 min. The flask was then filled with nitrogen after evacuation and heated to 340 °C, dissolving brown CdO and forming a colourless cadmium complex. The mixture was then cooled to 120 °C and continuously evacuated for at least 2 hours to remove water formed as a byproduct of Cd-ODPA complexation. After evacuation, the mixture was reheated to 370 °C. 0.4359 g of ~1.7 M Se dissolved in trioctylphosphine (TOP), and an additional 1.56 g of TOP are injected swiftly, and the reaction is stopped immediately by removing the heating mantle and decreasing the temperature. Then 5 mL toluene was added when the reaction mixture reached ~90 °C. The resulting product was then transferred to a nitrogen-filled glovebox. The CdSe seeds were then precipitated using a 10 mL, 1 : 1 toluene–methanol mixture and centrifuged at 4000 rpm for about 5 min. After at least three precipitation steps the CdSe seeds were re-dispersed in toluene and further used in synthesis.

CdSe@CdS nanorods were then synthesized using the literature protocol established by Amirav *et al.*[23] Briefly, CdO (0.2097 g), ODPA (~1.13 g), *n*-propylphosphonic acid (PPA, 65.75 mg) and TOPO (~3.33 g) were mixed in a three-neck flask. The flask was then heated to 80 °C to melt the reaction mixture under constant stirring. Then, the flask was heated to 120 °C and evacuated for 30 min. After that, the flask was flushed with N_2 atmosphere and heated further to 340 °C. At this temperature, 1.5 g TOP and 0.05 g sulphur dissolved in 0.60 g TOP was injected, and after 20 s, 2 mg of CdSe seeds dissolved in 0.5 g TOP was injected. The mixture was kept at a

constant temperature for 10 min until the colour of the solution turned from red to orange. After 10 min, the heating mantle was removed, and the reaction mixture was allowed to cool naturally. 5 mL of toluene was added once the temperature reached below 90 °C to dissolve the product and to transfer the product to a nitrogen-filled glovebox. To purify the thus obtained nanorods, equal amounts of toluene and methanol were added to precipitate the nanorods, and the mixture was centrifuged at 4000 rpm for 10 min. The precipitate was then mixed with hexane, 2 mL nonanoic acid and 2 mL octylamine to re-disperse. Next, the mixture was precipitated using methanol. The precipitation and dispersion steps were performed multiple times to purify the nanorods. A size exclusion step was performed twice using 10 mL toluene and 6 mL isopropyl alcohol mixture and centrifuged at 4000 rpm for 30 min. Finally, the nanorods were re-dispersed in toluene for further investigations.

Steady-state UV/vis absorption spectra were acquired using a JASCO V780 UV–visible/NIR spectrophotometer (JASCO GmbH, Pfungstadt, Germany). All measurements were performed in 1 cm quartz cuvettes in reference to pure solvent in the wavelength range 350–800 nm.

The TEM image of the nanorods, drop casted on a carbon coated copper grid, were collected using Hitachi HT7820 operating at 100 kV acceleration voltage in bright field mode.

The femtosecond-TA data was recorded using a home-built transient absorption setup with a detection system from Pascher Instruments AB. Briefly, a regenerative Ti:sapphire amplifier (Astrella, Coherent, USA) delivers pulses centred at 800 nm with ~100 fs full width at half maximum, 5 mJ pulse energy, and 1 kHz pulse repetition rate. The output fundamental is split into several beams. To generate the excitation pulses 2 mJ of the fundamental output of the amplifier are pumping an optical parametric amplifier (TOPAS, Light conversion, Lithuania) to produce tuneable pump pulses, and the second pump pulse was generated *via* second harmonic generation using a BBO crystal. For our experiments, both pump pulses of a central wavelength of 400 nm were used, with a typical beam diameter of 400–500 μm at the sample position, which is controlled every day to reliably calculate the intensity in μJ cm^{-2} for every experiment. A mechanical chopping scheme for the 1st pump pulse reduces the repetition rate to 500 Hz by blocking every other pulse, and another mechanical chopper for the 2nd pump pulse with 250 Hz, allowing two pulses to pass and blocking the next two pulses, is used to perform three pump–probe experiments in three different channels. One channel records the 1st pump–probe, the second one records the 2nd pump–probe, and the third channel records the pump–repump probe experiment simultaneously. Another part of the fundamental travels over a 2 ns delay line is focused onto a rotating CaF_2 window to generate a broadband white light continuum (300–700 nm), which is collimated using a parabolic mirror as a probe beam. The relative polarization of both, the pump and probe, is set to the magic angle of 54.7°. The spectra of probe and reference probe pulses are recorded by a CCD array detector after passing a Czerny–Turner spectrograph with a 150 mm focal length (SP2150, Princeton Instruments). The laser power was measured using a Gentec-EO (Canada) Maestro model connected to an XLP12-3S-VP-D0 thermal sensor, and the beam profiling was performed using a beam profiler, and the diameter of the pump beam was a $1/e^2$ distance from the highest intensity point. The obtained TA data was chirp-corrected and pre-processed using a Python-based package, KiMoPack.[37] The intensity-dependent ppp-TA data in the time range 2–1000 ps were fit using a slightly modified script published for target model sampling using the Markov Chain Monte Carlo method.[21] The script was modified to adapt our target model described in the main text and in the SI. The samples for the measurements were prepared in 1 mm sealed cuvettes to exclude exposure to moisture and oxygen.

Author contributions

The manuscript was written through the contributions of all authors. KK: Conceptualization, Methodology, Data Acquisition, Data Analysis, Writing - original draft. JU: Data Analysis, Discussion, Writing. RB: Data Analysis, Discussion, Writing. SY: Methodology, Data Acquisition, Writing. MW: Conceptualization, Resources, Supervision, Funding acquisition, Writing - original draft. All authors have given approval to the final version of the manuscript.

Conflicts of interest

The authors declare no competing financial interest.

Data availability

The data supporting this article is included in the article itself or as part of the supplementary information (SI). Supplementary information: absorption spectra and TEM images, details on the kinetic model, MCMC fits and concentration profiles. See DOI: https://doi.org/10.1039/d5nr04981d.

Acknowledgements

We thank the German Research Foundation (DFG) for supporting this work under project number 364549901-TRR234 CATALIGHT, TP B04 and project number 468735112 – KU 4220/1-1. J. U. acknowledges funding from VR Grant No. 2020-04995 and LINXS for this research.

References

1 D. V. Talapin, J.-S. Lee, M. V. Kovalenko and E. V. Shevchenko, Prospects of Colloidal Nanocrystals for

Electronic and Optoelectronic Applications, *Chem. Rev.*, 2010, **110**, 389–458.
2 S. V. Kershaw, L. Jing, X. Huang, M. Gao and A. L. Rogach, Materials aspects of semiconductor nanocrystals for optoelectronic applications, *Mater. Horiz.*, 2017, **4**, 155–205.
3 A. M. Smith and S. Nie, Semiconductor Nanocrystals: Structure, Properties, and Band Gap Engineering, *Acc. Chem. Res.*, 2010, **43**, 190–200.
4 J. M. Pietryga, Y.-S. Park, J. Lim, A. F. Fidler, W. K. Bae, S. Brovelli and V. I. Klimov, Spectroscopic and Device Aspects of Nanocrystal Quantum Dots, *Chem. Rev.*, 2016, **116**, 10513–10622.
5 N. Gaponik, S. G. Hickey, D. Dorfs, A. L. Rogach and A. Eychmüller, Progress in the light emission of colloidal semiconductor nanocrystals, *Small*, 2010, **6**, 1364–1378.
6 J. K. Stolarczyk, S. Bhattacharyya, L. Polavarapu and J. Feldmann, Challenges and Prospects in Solar Water Splitting and CO_2 Reduction with Inorganic and Hybrid Nanostructures, *ACS Catal.*, 2018, **8**, 3602–3635.
7 X.-B. Li, C.-H. Tung and L.-Z. Wu, Semiconducting quantum dots for artificial photosynthesis, *Nat. Rev. Chem.*, 2018, **2**, 160–173.
8 V. I. Klimov, Spectral and Dynamical Properties of Multiexcitons in Semiconductor Nanocrystals, *Annu. Rev. Phys. Chem.*, 2007, **58**, 635–673.
9 P. Kambhampati, Multiexcitons in Semiconductor Nanocrystals: A Platform for Optoelectronics at High Carrier Concentration, *J. Phys. Chem. Lett.*, 2012, **3**, 1182–1190.
10 C. A. Nelson, N. R. Monahan and X.-Y. Zhu, Exceeding the Shockley–Queisser limit in solar energy conversion, *Energy Environ. Sci.*, 2013, **6**, 3508.
11 X. Zhu, Exceeding the Limit in Solar Energy Conversion with Multiple Excitons, *Acc. Chem. Res.*, 2013, **46**, 1239–1241.
12 H. Zhu, Y. Yang and T. Lian, Multiexciton annihilation and dissociation in quantum confined semiconductor nanocrystals, *Acc. Chem. Res.*, 2013, **46**, 1270–1279.
13 S. L. Sewall, R. R. Cooney, E. A. Dias, P. Tyagi and P. Kambhampati, State-resolved observation in real time of the structural dynamics of multiexcitons in semiconductor nanocrystals, *Phys. Rev. B: Condens. Matter Mater. Phys.*, 2011, **84**, 235304.
14 R. J. Ellingson, M. C. Beard, J. C. Johnson, P. Yu, O. I. Micic, A. J. Nozik, A. Shabaev and A. L. Efros, Highly Efficient Multiple Exciton Generation in Colloidal PbSe and PbS Quantum Dots, *Nano Lett.*, 2005, **5**, 865–871.
15 R. D. Schaller and V. I. Klimov, High efficiency carrier multiplication in PbSe nanocrystals: Implications for solar energy conversion, *Phys. Rev. Lett.*, 2004, **92**, 1–4.
16 N. Lenngren, T. Garting, K. Zheng, M. Abdellah, N. Lascoux, F. Ma, A. Yartsev, K. Žídek and T. Pullerits, Multiexciton Absorption Cross Sections of CdSe Quantum Dots Determined by Ultrafast Spectroscopy, *J. Phys. Chem. Lett.*, 2013, **4**, 3330–3336.
17 H. Tahara, M. Sakamoto, T. Teranishi and Y. Kanemitsu, Quantum coherence of multiple excitons governs absorption cross-sections of PbS/CdS core/shell nanocrystals, *Nat. Commun.*, 2018, **9**, 3179.
18 K. E. Shulenberger, S. J. Sherman, M. R. Jilek, H. R. Keller, L. M. Pellows and G. Dukovic, Exciton and biexciton transient absorption spectra of CdSe quantum dots with varying diameters, *J. Chem. Phys.*, 2024, **160**, 014708.
19 R. Baruah, K. Kumar, J. Dellith and M. Wächtler, Tuning high-order multiexciton properties of colloidal CdSe quantum dots *via* size and surface modification, *Phys. Chem. Chem. Phys.*, 2025, **27**, 11066–11078.
20 K. Kumar and M. Wächtler, Spectral and dynamical properties of multiexcitons in semiconductor nanorods, *Nanoscale*, 2025, **17**, 7141–7152.
21 M. N. Ashner, S. W. Winslow, J. W. Swan and W. A. Tisdale, Markov Chain Monte Carlo Sampling for Target Analysis of Transient Absorption Spectra, *J. Phys. Chem. A*, 2019, **123**, 3893–3902.
22 L. Carbone, C. Nobile, M. De Giorgi, F. D. Sala, G. Morello, P. Pompa, M. Hytch, E. Snoeck, A. Fiore, I. R. Franchini, M. Nadasan, A. F. Silvestre, L. Chiodo, S. Kudera, R. Cingolani, R. Krahne and L. Manna, Synthesis and Micrometer-Scale Assembly of Colloidal CdSe/CdS Nanorods Prepared by a Seeded Growth Approach, *Nano Lett.*, 2007, **7**, 2942–2950.
23 L. Amirav and A. P. Alivisatos, Photocatalytic hydrogen production with tunable nanorod heterostructures, *J. Phys. Chem. Lett.*, 2010, **1**, 1051–1054.
24 Y. Ben-Shahar, J. P. Philbin, F. Scotognella, L. Ganzer, G. Cerullo, E. Rabani and U. Banin, Charge Carrier Dynamics in Photocatalytic Hybrid Semiconductor-Metal Nanorods: Crossover from Auger Recombination to Charge Transfer, *Nano Lett.*, 2018, **18**, 5211–5216.
25 K. Wu, W. E. Rodríguez-Córdoba, Z. Liu, H. Zhu and T. Lian, Beyond band alignment: Hole localization driven formation of three spatially separated long-lived exciton states in CdSe/CdS nanorods, *ACS Nano*, 2013, **7**, 7173–7185.
26 T. Labrador and G. Dukovic, Simultaneous Determination of Spectral Signatures and Decay Kinetics of Excited State Species in Semiconductor Nanocrystals Probed by Transient Absorption Spectroscopy, *J. Phys. Chem. C*, 2020, **124**, 8439–8447.
27 H. Zhu, N. Song, W. Rodríguez-Córdoba and T. Lian, Wave Function Engineering for Efficient Extraction of up to Nineteen Electrons from One CdSe/CdS Quasi-Type II Quantum Dot, *J. Am. Chem. Soc.*, 2012, **134**, 4250–4257.
28 Y. Liu, D. A. Cullen and T. Lian, Slow Auger Recombination of Trapped Excitons Enables Efficient Multiple Electron Transfer in CdS–Pt Nanorod Heterostructures, *J. Am. Chem. Soc.*, 2021, **143**, 20264–20273.
29 C. Müller, T. Pascher, A. Eriksson, P. Chabera and J. Uhlig, KiMoPack: A python Package for Kinetic Modeling of the Chemical Mechanism, *J. Phys. Chem. A*, 2022, **126**, 4087–4099.
30 V. I. Klimov, A. A. Mikhailovsky, D. W. McBranch, C. A. Leatherdale and M. G. Bawendi, Quantization of mul-

tiparticle Auger rates in semiconductor quantum dots, *Science*, 2000, **287**, 1011–1014.

31 V. I. Klimov, J. A. McGuire, R. D. Schaller and V. I. Rupasov, Scaling of multiexciton lifetimes in semiconductor nanocrystals, *Phys. Rev. B: Condens. Matter Mater. Phys.*, 2008, **77**, 195324.

32 Z.-J. Jiang and D. F. Kelley, Hot and Relaxed Electron Transfer from the CdSe Core and Core/Shell Nanorods, *J. Phys. Chem. C*, 2011, **115**, 4594–4602.

33 M. G. Lupo, F. D. Sala, L. Carbone, M. Zavelani-Rossi, A. Fiore, L. Lüer, D. Polli, R. Cingolani, L. Manna and G. Lanzani, Ultrafast electron-hole dynamics in core/shell CdSe/CdS Dot/Rod nanocrystals, *Nano Lett.*, 2008, **8**, 4582–4587.

34 N. Lenngren, T. Garting, K. Zheng, M. Abdellah, N. Lascoux, F. Ma, A. Yartsev, K. Žídek and T. Pullerits, Multiexciton Absorption Cross Sections of CdSe Quantum Dots Determined by Ultrafast Spectroscopy, *J. Phys. Chem. Lett.*, 2013, **4**, 3330–3336.

35 K. E. Shulenberger, S. J. Sherman, M. R. Jilek, H. R. Keller, L. M. Pellows and G. Dukovic, Exciton and biexciton transient absorption spectra of CdSe quantum dots with varying diameters, *J. Chem. Phys.*, 2024, **160**, 014708.

36 L. Carbone, C. Nobile, M. De Giorgi, F. D. Sala, G. Morello, P. Pompa, M. Hytch, E. Snoeck, A. Fiore, I. R. Franchini, M. Nadasan, A. F. Silvestre, L. Chiodo, S. Kudera, R. Cingolani, R. Krahne and L. Manna, *Nano Lett.*, 2007, **7**, 2942–2950.

37 C. Müller, T. Pascher, A. Eriksson, P. Chabera and J. Uhlig, *J. Phys. Chem. A*, 2022, **126**, 4087–4099.